


Optimal Estimation of Secondary Flow Coefficient in Compound Channels with Vegetated Floodplains

Marzieh Mohseni^{1*}, Amineh Naseri²

1- Assistant Professor, Department of Civil Engineering, Sirjan University of Technology, Sirjan, Iran.

2- Instructor, Department of Computer Engineering, Sirjan University of Technology, Sirjan, Iran.

* Mohseni_m@sirjantech.ac.ir

Received: 7 June 2022, Accepted: 10 August 2022  J. Hydraul. Homepage: www.jhyd.iha.ir

Abstract

This study adopted the Shiono-Knight model (SKM) to estimate the lateral distribution of the depth-averaged velocity within rectangular and trapezoidal compound channels with emergent vegetation in floodplains. To implement the SKM, it was required to estimate the eddy viscosity coefficient, friction coefficient, and secondary flow coefficient. The present study estimated the friction coefficient using the Colebrook–White equation modified by Rameshwaran and Shiono for vegetated beds. An analysis of eddy viscosity models across compound channels indicated that the model was not sensitive to the eddy viscosity coefficient; thus, the eddy viscosity coefficient could be assumed constant across the channel. However, the negligence of the secondary flow in the model would lead to a significant error, and it was required to calibrate the secondary flow coefficient. Thus, this study used a genetic algorithm (GA) to develop equations for the secondary flow coefficient for different sections of the compound channel under two different approaches: (1) the approach of Abril and Knight (2004), who proposed constant values for the main channel and floodplains, and (2) the equations of Devi and Khatua (2017), which related the secondary flow coefficient to the relative depth and width ratio. It was found that the secondary flow coefficient was dependent on the relative depth and width ratio. As a result, the equation optimized based on the Devi-Khatua approach outperformed the Rameshwaran-Shiono technique in estimating the lateral distribution of the velocity, with a 10.2% lower error.

Keywords: Depth-averaged velocity, Emergent, Shiono-Knight model, Genetic Algorithm, Relative depth, Width ratio.



© 2024 Iranian Hydraulic Association, Tehran, Iran.
This is an open access article distributed under the terms and conditions of
the Creative Commons Attribution 4.0 International (CC BY 4.0 license)
(<http://creativecommons.org/licenses/by/4.0/>)

1. Introduction

Natural rivers are typically described as a compound channel consisting of a main channel to transport the primary flow and a floodplain to transport the extra flow during a flood event. Moreover, open channels are often designed and constructed in a compound form in many hydraulic projects to enhance the stability of channel slopes and discharge capacity (Alawadi et al., 2018). The differences in the flow depth and bed roughness in main channel and floodplain lead to a significant gradient in the lateral velocity distribution within a compound channel. As a result, a strong lateral shear stress layer results in mass and momentum exchanges between the main channel and floodplain. An important consequence of the momentum exchange is the reduction of discharge capacity of the river compared to a situation in which the channel and the floodplain are considered as separated channels. This phenomenon is referred to as the kinematic effect (Yang et al., 2007).

Primary experimental tests indicated that the single-channel method and divided channel method were not highly accurate in the transport capacity prediction of compound channels (Posey, 1967; Sellin, 1964; Zheleznyakov, 1971). Later, studies focused on the interaction between the main channel and floodplain and boundary shear stress distribution (Rajaratnam and Ahmadi, 1979; Knight and Hamed, 1984; Knight et al., 1994). Numerous empirical studies have been conducted on straight compound channels with or without floodplain vegetation to identify the flow mechanisms in the past three decades. Shiono and Knight (1990) accurately studied flow characteristics and Reynolds shear stresses between the main channel and floodplain within a large-scale flume and proposed an analytical model to predict the depth-averaged velocity distribution and boundary shear stress in a prismatic compound channel. The Shiono-Knight model (SKM) is a lateral distribution model (LDM) that incorporates secondary flow and eddy viscosity parameters. Similar studies were later conducted (Abril and Knight, 2004; Bousmar and Zech, 2004; Tang and Knight, 2009; Das et al., 2018).

In general, common analytical models were used to calculate the depth-averaged velocity are mostly based on SKM. SKM uses three

hydraulic parameters, including the friction coefficient f , eddy viscosity coefficient λ , and secondary flow parameter Γ , to describe all the energy dissipation-related mechanisms in three-dimensional flows (Alawadi, 2018). A number of studies recently calibrated the SKM parameters for simple and compound channels. Abril and Knight (2004) introduced a simple method to calibrate the three SKM parameters. They also demonstrated that the secondary flow parameter could be assumed proportionate to the gravity term, proposing a constant secondary flow coefficient k .

Lashkarara and Dehghani (2016) calibrated the friction coefficient, secondary flow parameter, and eddy viscosity coefficient using experimental data and earlier works through evolutionary optimization to obtain the shear stresses in different sections of the compound channel. The results indicated that the friction coefficient and eddy viscosity coefficient underwent relatively substantial changes at p_b/p_w ratios below 4, the p_b/p_w ratio, in which p_b and p_w denote the wetted perimeters of the channel bed and wall, respectively (Lashkar Ara and Dehghani, 2016). It was demonstrated that the calibration of the proposed secondary flow coefficient equations would contribute to SKM performance improvement in compound channels.

Devi and Khatua (2017) proposed equations based on experimental data to define the secondary flow coefficient as a function of the relative depth D_r and width ratio W_r , the relative depth was defined as the ratio of the floodplain flow depth to the flow depth in the main channel, and the width ratio was assumed to be the ratio of the total compound channel width to the bed width of the main channel. Alwadi et al. (2018) calibrated the secondary flow coefficients according to the Devi and Khatua (2017) approach. They concluded that the secondary flow coefficients depend on width ratio and relative depth. Moreover, the application of the Devi and Khatua (2017) approach would have appropriate results.

Furthermore, due to desirable moisture conditions, floodplains often have full or partial vegetation (Tang and Knight, 2009). Vegetation serves as a barrier and increases turbulence, influencing the flow depth, velocity distribution, and sediment transport (Pu et al., 2019).

The effect of vegetation on flow characteristics is dependent on vegetation type in terms of,

rigidity or flexibility, leave-to-stem surface ratio, vegetation pattern, density, and stem diameter (Han et al., 2016).

Understanding the hydraulic of the flow in a compound channel with vegetation on floodplains for determining the stage-discharge curve, river management and river ecosystem projects is of considerable importance (Yang and Knight, 2007). Several empirical studies have been conducted on vegetated channels in recent years. They highlighted the influence of the submersion degree, density, and vegetation pattern on the flow structure and lateral shear stress. Pasche and Rouve(1985) pioneered the theoretical and experimental evaluation of flow characteristics in compound channels. They explored the effects of emergent roughness on flow characteristics, such as vortex formation and momentum exchange, in the floodplain. The depth-averaged velocity profile was studied for different vegetation types, such as trees, shrubs, and grass, under emergent and submerged conditions by Yang et al., (2007). Sun and Shiono (2009) measured the velocity and boundary shear stress within a straight compound channel with a row of vegetation along the floodplain. The experimental work of Sun and Shiono led to the development of several quasi-2D models to predict the lateral velocity distribution and shear stress in the presence of vegetation (Tang and Knight, 2009; Sun et al., 2013; Liu et al., 2013). Rameshwaran and Shiono estimated the lateral velocity distribution and bed shear stress distribution within compound channels with a vegetated floodplain by adding the drag force to the Reynolds-averaged Navier–Stokes (RANS) equations and numerically solving it. They showed that the secondary flow parameter in a compound channel with a vegetated floodplain would be substantially higher than that in a channel with a non-vegetated floodplain. This study used the modified Colebrook–White equation to calculate the friction coefficient under a floodplain with vegetation. Five eddy viscosity models proposed in earlier works were adopted, and the optimal model was found to be a combination of the bed turbulence model and shear stress (Rameshwaran and Shiono, 2007).

The present study aims to evaluate the performance of SKM in the prediction of the depth-averaged velocity within rectangular and

trapezoidal compound channels with different width ratios and floodplain vegetation patterns. Rarely were such channels studied in the SKM literature. As mentioned, the secondary flow parameter significantly influences the performance of SKM. Therefore, this study sought to develop equations to predict the secondary flow parameter based on a wide range of experimental data and using genetic algorithm (GA).

2. Materials and Methods

2.1. Theoretical foundations of SKM

To reflect the drag force of emergent vegetation on the flow, an additional momentum term is typically incorporated into the RANS equations in the form of a sink term. Tang and Knight proposed a depth-averaged RANS equation to measure the effect of emergent floodplain vegetation on the flow as (Tang and Knight, 2009):

$$\begin{aligned} \rho g H S_0 - \rho \frac{f}{8} U_d^2 \sqrt{1 + \frac{1}{s^2}} \\ + \frac{\partial}{\partial y} \left\{ \rho \lambda H^2 \left(\frac{f}{8} \right)^{1/2} U_d \frac{\partial U_d}{\partial y} \right\} \\ - \frac{1}{2\delta} \rho (C_D S_F A_p) H U_d^2 = \Gamma \end{aligned} \quad (1)$$

where ρ is the fluid density, g is the gravitational acceleration, S_0 is the channel bed slope in the flow direction, f is the bed friction coefficient, U_d is the depth-averaged velocity, H is water depth and s is the side slope of the banks (1:s, vertical:horizontal, as shown in Fig. 2). This model assumes vegetation as a rigid cylinder with a diameter of D_v . The vegetation characteristics included vegetation porosity δ , drag coefficient C_D , shading factor S_F , and A_p is the projected area of i plants per unit volume. Furthermore, y is the coordinate in the channel width direction, λ is the dimensionless eddy viscosity, and Γ is the secondary flow parameter. Shiono and Knight(1990) showed that the secondary flow parameter almost linearly changed in the channel width direction. These parameters were discussed for non-vegetated channels by Knight and Shiono (1996); Abril and Knight (2004); and Tominaga and Knight (2006) and for vegetated channels by Rameshwaran and Shiono (2007).

2.1.1. Analytical solving of the depth-averaged flow equation

Eq. (1) can be solved to obtain the depth-averaged velocity as a function of the channel width analytically (Shiono and Knight, 1990; Bousmar and Zech, 2004) or numerically (Abril and Knight, 2004; Knight and Abril, 1996). The SKM divided the cross-section of the channel into sub-sections based on the flow depth change (e.g., constant depth and linearly changing depth), proposing a depth-averaged velocity equation for each sub-section:

-The non-vegetated sub-section with a constant depth and a flat bed ($s = \infty$):

$$U_d = [A_1 e^{\gamma y} + A_2 e^{-\gamma y} + k]^{1/2} \quad (2)$$

$$k = \frac{8gS_0H}{f/8} (1 - \beta) \quad (3)$$

$$\gamma = \sqrt{\frac{2}{\lambda} \left(\frac{8}{f}\right)^{1/4} \frac{1}{H} \sqrt{\frac{f}{8}}} \quad (4)$$

$$\beta = \frac{\Gamma}{\rho g S_0 H} \quad (5)$$

-The non-vegetated sub-section with a linearly varying side bed ($s:1$):

$$U_d = [A_3 \xi^\alpha + A_4 \xi^{-(\alpha+1)} + \omega \xi + \eta]^{1/2} \quad (6)$$

where

$$\alpha = -\frac{1}{2} + \frac{1}{2} \sqrt{1 + \frac{s\sqrt{1+s^2}}{\lambda} \sqrt{8f}} \quad (7)$$

$$\omega = \frac{gS_0}{\frac{\sqrt{1+s^2}}{s} \left(\frac{f}{8}\right) - \frac{\lambda}{s^2} \sqrt{f/8}} \quad (8)$$

$$\eta = \frac{-\Gamma}{\rho \sqrt{1 + \frac{1}{s^2} \left(\frac{f}{8}\right)}} \quad (9)$$

-The vegetated sub-section with a constant depth ($s = \infty$):

$$U_d = [A_5 e^{\gamma y} + A_6 e^{-\gamma y} + k]^{1/2} \quad (10)$$

where

$$k = \frac{8gS_0H}{f/8 + C_D S_F A_v H / (2\delta)} (1 - \beta) \quad (11)$$

$$\gamma = \sqrt{\frac{2}{\lambda} \left(\frac{8}{f}\right)^{1/4} \frac{1}{H} \sqrt{\frac{f}{8} + \left(\frac{H}{2\delta}\right) C_D S_F A_v}} \quad (12)$$

$$\beta = \frac{\Gamma}{\rho g S_0 H} \quad (13)$$

where ξ is the local depth; $\xi = H + (y + b)/s$ for $y > 0$ and $\xi = H - (y - b)/s$ for $y < 0$, H is water depth and b is the half main channel bed width as shown in Fig. 2(b).

2.1.2. Boundary conditions in the analytical model

Unknown coefficients A_1 - A_6 in Eqs. (2), (6), and (10) can be obtained using suitable boundary conditions:

- 1) Non-slip condition; i.e., $U_d = 0$ on fixed boundaries. In the majority of studies, the “no-slip condition” is considered for the boundary condition at the wall, for instance, Tang and knight (2009) and Huai et al. (2009) used this boundary condition in their studies. However, Shiono et al. (2012) revealed that this boundary condition would not give an accurate velocity distribution near the walls, especially in narrow channels. Therefore, an appropriate value for the wall velocity obtains better results. Sun and Shiono (2008) showed that estimation an appropriate value of velocity at near the wall using either the lag-law or 7th power law as a boundary condition prevents the sharp changes of the velocity distribution near the wall. In this condition, the velocity at the wall is calculated using the mean boundary shear stress proportion to the wall shear stress with the Darcy friction equation $U_{wall}^2 = 0.75 R g S_0 / (f/8)$. In the vegetated region, the velocity at the wall is calculated using the ratio of the mean boundary shear stress proportion to the drag force per unit area, following this equation: $U_{wall}^2 = R g S_0 / (0.5 * C_D * N_v * H * D_v)$, where R is hydraulic radius (Mohseni, 2015).
- 2) Continuity of U_d in the interval of two subsections; i.e., $U_d^{(i)} = U_d^{(i+1)}$
- 3) Continuity of unit force $H \bar{\tau}_{yx}$ in the interval of two sub-sections; i.e., $[H \bar{\tau}_{yx}]^{(i)} = [H \bar{\tau}_{yx}]^{(i+1)}$. This can be written as:

$$\left(\mu \frac{\partial U_d}{\partial y}\right)^{(i)} = \left(\mu \frac{\partial U_d}{\partial y}\right)^{(i+1)} \text{ with } \mu = \lambda \sqrt{f} \quad (14)$$
- 4) The velocity gradient should be zero at the main channel centerline of the compound

channel (i.e., $\frac{\partial U_d}{\partial y} = 0$); superscript i represents the sub-section number.

2.1.3. Input model parameters for the analytical solving of SKM

To analytically solve SKM and estimate the lateral velocity distribution, it is required to estimate the drag coefficient, shading factor, friction coefficient, secondary flow parameter, and eddy viscosity coefficient.

- Friction coefficient

The wake created by stems induces a complex flow pattern in a vegetated floodplain, and the depth-averaged velocity profile deviates from the 3D logarithmic profile assumed in the Colebrook–White equation. Therefore, the modified Colebrook–White equation is employed. Rameshwaran and Shiono (2007) showed that the friction coefficient could be calculated using Eqs. (15a) and (15b) well agreed with the experimental:

$$f = [-2 \log \left[\frac{3.02\theta}{\sqrt{128gH^3S_0 + \frac{k_s}{12.3H}}} \right]]^{-2} \quad (15a)$$

$$f = [-2 \log \left[\frac{3.02\theta}{\sqrt{128gH^3S_0 + \frac{k_s}{1.2H}}} \right]]^{-2} \quad (15b)$$

Eqs. (15a) and (15b) are for smooth channels and vegetated floodplains respectively. The equivalent sand roughness height, k_s can be calculated as (Ackers, 1991):

$$k_s = (8.26\sqrt{gn})^6 \quad (16)$$

where n is the manning coefficient.

- Bulk drag coefficient

For an array of rods, the wake created by upstream rods reduces the drag coefficient on the downstream rods. Nepf (1999) demonstrated that this effect increased as the longitudinal and lateral distances between the rods reduced. The present study obtained the bulk drag coefficient using the wake interference model.

- Porosity

The obstruction effect of vegetation on the flow was defined based on the porosity parameter:

$$\delta = 1 - \sum (N_v A_v)_i \quad (17)$$

where A_v is the average cross-sectional area of stem i , while N_v is the number of plants per unit area ($1/m^2$).

- Eddy viscosity

Earlier works proposed various eddy viscosity models to predict the momentum exchange in the mixing layer, as shown in Table 1; Model 1 defines a constant eddy viscosity coefficient of $\kappa/6$ across the channel, while Models 2 and 3 assume the viscosity coefficient to be $\kappa/6$ in the main channel and a function of the relative depth in the floodplain.

Table 1. Eddy viscosity models

Models	Eddy viscosity	Coefficients	Eddy viscosity constant
Model 1 (Rameshwaran and Shiono, 2007)	$v_t = \lambda \sqrt{\frac{f}{8}} \bar{U}_d H$	$\lambda_{mc} = \kappa/6$ $\lambda_{fp} = \lambda_{mc}$	$\lambda_{mc} = 0.0683$ $\lambda_{fp} = 0.0683$
Model 2 (Shiono and Knight, 1991)	$v_t = \lambda \sqrt{\frac{f}{8}} \bar{U}_d H$	$\lambda_{mc} = \kappa/6$ $\lambda_{fp} = \lambda_{mc} (2D_r)^{-4}$	$\lambda_{mc} = 0.0683$
Model 3 (Abril and Knight, 2004)	$v_t = \lambda \sqrt{\frac{f}{8}} \bar{U}_d H$	$\lambda_{mc} = \kappa/6$ $\lambda_{fp} = \lambda_{mc} (-2.0 + 1.2D_r)^{-1.44}$	$\lambda_{mc} = 0.0683$

- Secondary flow parameter

The calibration of the secondary flow parameter is typically more difficult than that of the friction coefficient and eddy viscosity coefficient. However, Shiono and Knight (1990) showed that the secondary flow gradient was constant in different sections of a compound channel, and a constant secondary flow parameter could be defined for each individual section. This study adopted two approaches to the secondary flow parameter (Abril and Knight, 2004; Devi and Khatua, 2017). Abril and Knight's approach is based on the theoretical concept that relates the boundary shear stress and the secondary flow to each other, they also showed that the secondary flow term can be considered proportional to the gravitational term. They proposed the secondary flow coefficient (k) as a proportionality constant and finally presented two simple equations as:

$$\Gamma_{mc} = k_{mc} \rho g H S_0 \quad (18)$$

$$\Gamma_{fp} = k_{fp} \rho g H S_0 \quad (19)$$

$$\Gamma_s = k_s \rho g H S_0 \quad (20)$$

where k is the secondary flow coefficient, and subscripts mc , fp , and s , respectively represent to the main channel, floodplain, and the side slope region in a trapezoidal compound channel.

Earlier works proposed different secondary flow coefficients, Abril and Knight (2004) proposed $\Gamma/[\rho g H S_0] = 0.15$ and -0.25 for the main channel and non-vegetated floodplain. However, Rameshwaran and Shiono (2007) utilized experimental data and proposed $\Gamma/[\rho g H S_0] = 1.2Dr$ and $\Gamma/[\rho g(H-h)S_0] = 0.6Dr$ for the main channel and a vegetated floodplain, respectively. Here, $Dr = (H-h)/H$ is the relative depth. The second approach was developed by Devi and Khatua (2017) based on a wide range of experimental data from compound channels with a non-vegetated floodplain at different relative depths and width ratios. It exploits the average shear stress (τ_{avg}) in each section and the driving force per unit wetted area ($\rho g H S_0$) to calculate the secondary flow parameter. For each section, the secondary flow parameter is given by:

$$\Gamma_{mc} = \rho g H S_0 - \tau_{avgmc} \quad \text{or} \quad (21)$$

$$\Gamma_{mc} = \rho g H S_0 (1 - k'_{mc})$$

$$\Gamma_{fp} = \rho g H S_0 - \tau_{avgfp} \quad \text{or} \quad (22)$$

$$\Gamma_{fp} = \rho g H S_0 (1 - k'_{fp})$$

where

$$k'_{mc} = \frac{\tau_{avgmc}}{\rho g H S_0}, \quad k'_{fp} = \frac{\tau_{avgfp}}{\rho g H S_0} \quad (23)$$

From the comparison of equations 21 and 22 with equations 18 and 19, it can be concluded that $k = 1 - k'$.

For the side slope region in a trapezoidal compound channel the k'_s value is defined as:

$$k'_s = \frac{\tau_{avgs}}{\rho g H' S_0} \quad (24)$$

where H' is the average flow depth of side slope region.

Drawing on multivariate regression, Devi and Khatua (2017) calculated the secondary flow coefficient based on the dimensionless relative depth and width ratio as:

$$k'_{mc} = -0.5 + 0.45e^{-0.66Dr} + 1.1Wr^{-0.38} \quad (25)$$

$$k'_{fp} = 0.18 + 0.79e^{-0.28Dr} - 0.013Wr \quad (26)$$

$$k'_s = 0.01 - 0.474Dr + 2.06Wr^{-0.4} \quad (27)$$

The present study re-writes the equations of Devi and Khatua(2017) for compound channels consisting of a floodplain with emergent vegetation as:

$$k'_{mc} = (pr(1) * Dr^{0.0235}) + (pr(2) * Wr^{pr(3)}) \quad (28)$$

$$k'_{fp} = (pr(4) * Dr^{pr(5)}) + (pr(5) * Wr^{pr(6)}) \quad (29)$$

$$k'_s = (pr(7) * Dr^{pr(8)}) + (pr(9) * Wr^{pr(10+)}) \quad (30)$$

where the unknown coefficients and exponents were calculated based on the minimum error between the experimental data and SKM output. This study employed a GA for optimization and the estimation of the unknown parameters.

2.2. GA

GAs are a class of computational models inspired by Darwin's theory of evolution that the survival of a living creature is influenced by the survival of the strongest species. These algorithms code the feasible solutions to a given problem in a chromosome-like structure of data and apply crossover operators to maintain vital information in these structures. GAs are often known as function optimizers; however, GAs can be employed in a wide range of applications. A GA is typically implemented by generating a population of chromosomes. Then, the generated data structures (i.e., chromosomes) are evaluated, with those better representing the optimal solution to the problem having a higher reproduction probability than weaker solutions. The goodness of a solution is usually measured relative to the current population of candidate solutions. In the search for the optimal solution, an initial population of solutions is created. Then, a set of varied solutions is generated in successive generations – in each generation of the GA, particular changes occur in the chromosome genes of the population. The initial solutions often change such that the

solution population converges to the optimal solution in each generation. A number of chromosomes in the population are exchanged through a crossover, generating new chromosomes of offspring with a combination of the genes of their parents. Several chromosomes undergo mutation in their genes in each generation. The number of chromosomes undergoing a crossover or mutation is controlled by the crossover and mutation rates. The population chromosomes maintained for the next generation are selected based on Darwin's theory of evolution; i.e., chromosomes of a higher fit are more likely to be in the next generation. The chromosomes converge to a certain value after a number of generations, which represents the optimal solution to the problem. The process of a GA can be summarized as a continuous shift from a candidate solution population (chromosomes) to a new population of fitter solutions based on natural selection through crossover and mutation operators. This evaluation-selection-reproduction cycle

continues until an optimal or near-optimal solution is found (Zahiri et al., 2017).

2.2.1. Objective functions and decision variables

The decision variables included the coefficients and exponents in Eqs. (28-30). To find the optimal values of these variables, the root-mean-square error (RMSE) can be used.

where U_{d-SKM} and U_{d-Exp} denote the observed and predicted depth-averaged velocities, respectively, and n is the total number of depth-averaged velocity data points within the compound channel. The GA was employed to implement this minimization and find the optimal coefficients and exponents $pr(i)$ in Eqs. (28-30). RMSE can be equal to or larger than zero. However, the ideal RMSE is zero. Fig. 1 illustrates the flowchart of the proposed model.

$$f(x) = \min \left(\sqrt{\frac{\sum (U_{(d-SKM)} - U_{(d-Exp)})^2}{n}} \right) \quad (31)$$

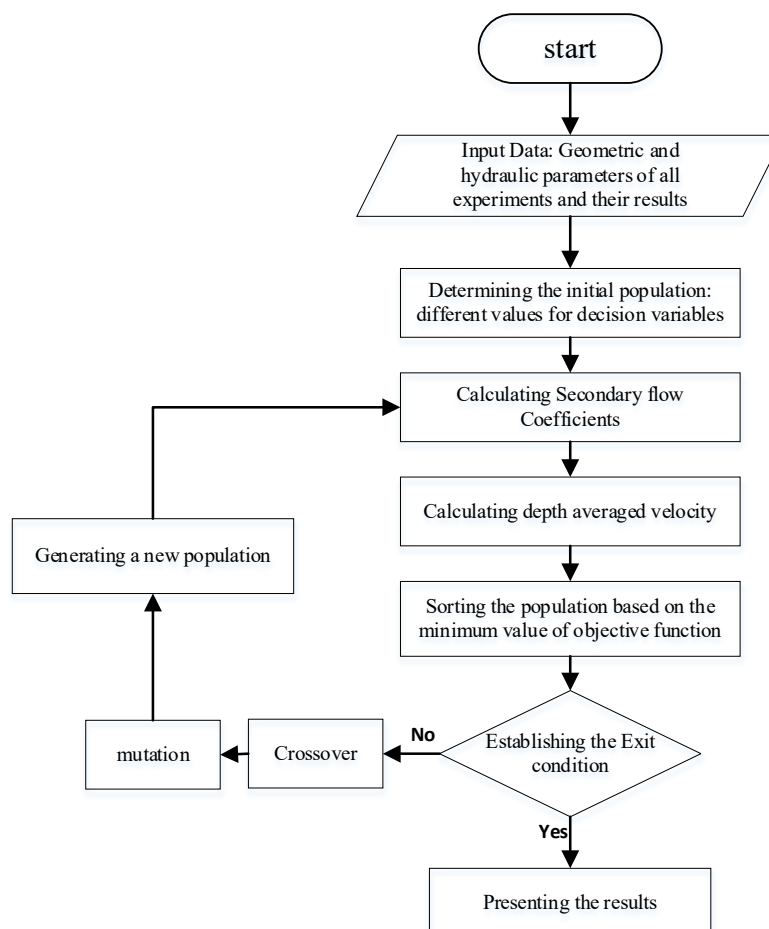


Fig. 1 The flowchart of the proposed model

Table 2. Summary of experimental conditions used in the proposed model.

Sources	Cases	H(m)	h(m)	Dr	b(m)	B(m)	S ₀	sm	Dv(m)	Ln(m)	ls(m)	Notes
Tavakoli and Mohseni (2020)	Sh 10-0.29	0.09	0.06	0.29	0.12	0.4	0.0012	0	0.007	0.1	0.1	symmetric
	Sh 10-0.4	0.1	0.06	0.4	0.12	0.4	0.0012	0	0.007	0.1	0.1	
	Sh 10-0.5	0.12	0.06	0.5	0.12	0.4	0.0012	0	0.007	0.1	0.1	
	Sh 5-0.29	0.089	0.06	0.29	0.12	0.4	0.0012	0	0.007	0.05	0.05	
	Sh 5-0.4	0.11	0.06	0.4	0.12	0.4	0.0012	0	0.007	0.05	0.05	
	Sh 5-0.5	0.12	0.06	0.5	0.12	0.4	0.0012	0	0.007	0.05	0.05	
	Sh 2.5-0.29	0.085	0.06	0.29	0.12	0.4	0.0012	0	0.007	0.025	0.025	
	Sh 2.5-0.4	0.10	0.06	0.4	0.12	0.4	0.0012	0	0.007	0.025	0.025	
	Sh 2.5-0.5	0.165	0.06	0.5	0.12	0.4	0.0012	0	0.007	0.025	0.025	
Mohseni (2015)	S1-1	0.083	0.06	0.27	0.08	0.3	0.001	1.333	0.006	0.03	0.02	asymmetric
	S1-2	0.094	0.06	0.36	0.08	0.3	0.001	1.333	0.006	0.03	0.02	
	S1-3	0.12	0.06	0.5	0.08	0.3	0.001	1.333	0.006	0.03	0.02	
	S1-4	0.083	0.06	0.27	0.08	0.3	0.002	1.333	0.006	0.03	0.02	
	S1-5	0.094	0.06	0.36	0.08	0.3	0.002	1.333	0.006	0.03	0.02	
	S1-6	0.12	0.06	0.5	0.08	0.3	0.002	1.333	0.006	0.03	0.02	
	S1-7	0.083	0.06	0.27	0.08	0.3	0.004	1.333	0.006	0.03	0.02	
	S1-8	0.094	0.06	0.36	0.08	0.3	0.004	1.333	0.006	0.03	0.02	
	S1-9	0.12	0.06	0.5	0.08	0.3	0.004	1.333	0.006	0.03	0.02	
Rameshwaran and Shiono (2007)	FCF070201	0.1655	0.15	0.094	0.75	3.15	0.001027	1	0.025	0.2685	0.31	symmetric
	FCF070301	0.1765	0.15	0.15	0.75	3.15	0.001027	1	0.025	0.2685	0.31	
	FCF070401	0.1859	0.15	0.19	0.75	3.15	0.001027	1	0.025	0.2685	0.31	

2.3. Experimental data

A total of 21 experimental data series reported by Rameshwaran and Shiono (2007), Tavakoli and Mohseni (2020), and Mohseni et al. (2013) were exploited to find the optimal coefficients and exponents $pr(i)$ in Eqs. (28-30). These three channels had symmetric and asymmetric cross-sections with different emergent vegetation patterns and densities in the floodplain. Table 2 summarizes the channels and experimental setup. Further details on the channels and experiments are available in earlier works (Rameshwaran and Shiono, 2007; Tavakoli and Mohseni, 2020; Mohseni et al., 2013).

The model was first applied to the symmetric compound channel with emergent vegetation fully covered on the floodplain, built in the Flood Channel Facility (FCF) at Wallingford, UK. The experimental set up for the UK-FCF series B programme is briefly described here and is detailed in Rameshwaran and Shiono (2007). The main channel and

floodplain had a width of 0.75 and 2.25 m, respectively. Furthermore, s_m and s_f (both 1.0), denote the main channel side wall slope distance and the floodplain side wall slope distance, respectively. Bankfull depth h is 0.15 m and channel has a constant bed slope of $S_0=1.027 \times 10^{-3}$. The channel surfaces were flat cementitious mortar, and the floodplain was covered with vertical straight wooden rods on a smooth surface. The vegetation was assumed to have a diameter of $D_v=0.025$ m and a density of twelve stems per unit area (m^2). Table 2 summarizes the setup (Rameshwaran and Shiono, 2007). As the channel was symmetric, only half of it was modeled. It was divided into a main channel, bank of main channel, vegetated floodplain, and bank of floodplain, as shown in Fig. 2(a).

The asymmetric compound channel with emergent vegetation on the floodplain used by Mohseni (2015) was constructed in a 10 m long, 0.3 m wide and 0.4 m high plexiglass tilting flume in the hydraulics laboratory of Tarbiat Modares University, Iran. The main

channel and floodplain had widths of 0.08 m and 0.14 m, respectively, and the bank slope of the main channel was 1.33. The bankfull height h was 0.06 m. Circular rods with a diameter of 0.006 m were installed on the floodplain at a spacing of 0.03 m in the longitudinal direction and 0.02m in the lateral direction to represent emergent floodplain vegetation. To perform the SKM, the channel was divided into the main channel, the bank slope region, and a vegetated floodplain, as shown in Fig. 2(b). It should be mentioned, that the experimental flume which used by Mohseni (2015) was a narrow flume, which had no suitable results with no-slip conditions, therefore, the velocity at the wall has been used for the boundary condition at the wall.

Tavakoli and Mohseni (2020) studied an experimental flume with a plexiglass bed and walls. It had a length of 10 m, a width of 0.8 m, and a constant slope of 0.00012 at the Hydraulics Laboratory of the Sirjan University of Technology, Iran. They implemented a symmetric compound channel with emergent vegetation across the floodplain, as shown in Fig. 2(c). The main channel had a width of 0.24 m, a slope of 0, and an bankfull depth of 0.06 m. Circular straws were employed at a spacing of 0.025, 0.05, and 0.1 m to represent floodplain vegetation. To implement the SKM, the channel was divided into two sections, i.e., the main channel and a vegetated floodplain, as shown in Fig. 2(c).

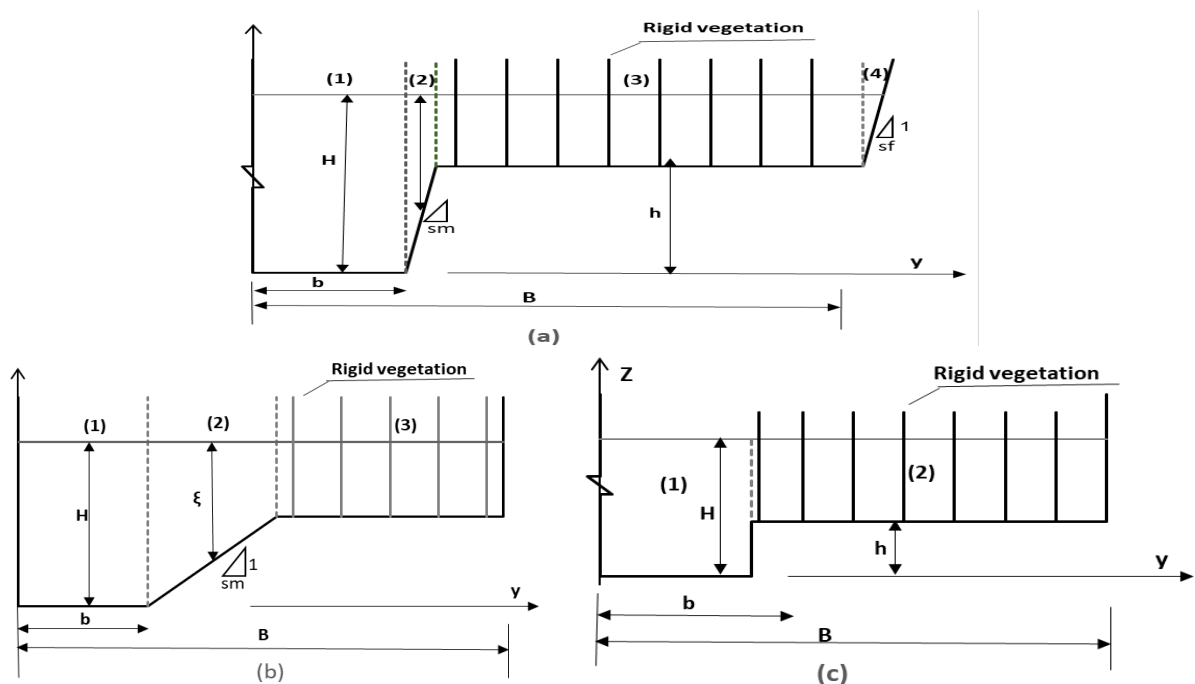


Fig. 2 Different types of vegetated compound channels used (a) Symmetric compound channels with emergent vegetation on the floodplain by Rameshwaran and Shiono (2007), (b) Asymmetric compound channels with emergent vegetation on the floodplain by Mohseni (2015), (c) Symmetric compound channels with vegetation on the floodplain by Tavakoli and Mohseni (2020).

3. Results and Discussion

3.1. Eddy viscosity models

Several models have been proposed to estimate the eddy viscosity coefficient within a compound channel (Table 1). A number of such models assume a constant eddy viscosity coefficient along the channel, while some others define different viscosity coefficients for the main channel and floodplain. The effects of the eddy viscosity coefficient on the model output were explored while the other

parameters were fixed, as shown in Fig. 3. The mean absolute percentage error (MAPE) was employed as the evaluation criterion for the eddy viscosity models. MAPE was obtained to be 0.285, 0.288, and 0.293 for Models 1, 2, and 3, respectively. It was found that the eddy viscosity coefficient had no significant influence on the depth-averaged velocity estimate. Hence, a constant eddy viscosity coefficient of 0.0683 was applied across the channel. This was verified by Liu et al. (2013).

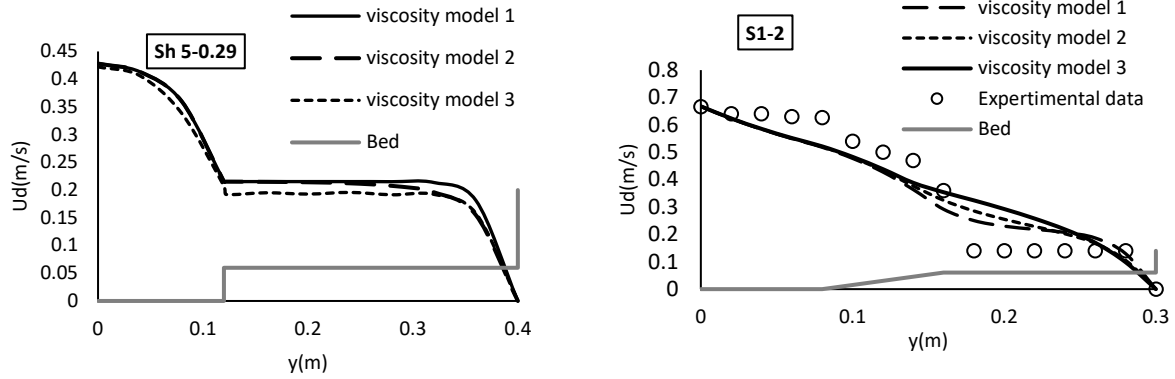


Fig. 3 Comparison of Depth averaged velocity (U_d) for different eddy viscosity models

3.2. Secondary flow coefficient

A code was written in MATLAB to implement the SKM and GA. To estimate the secondary flow parameter, 15 of the 21 data points were employed. The remaining 6 data points were used to validate the model. The population size, crossover rate, and mutation rate strongly affect the performance of a GA. The optimal population size and crossover and mutation rates were calculated to be 200, 0.8, and 0.2 through trial and error, respectively.

Eqs. (32-34) were obtained to calculate the secondary flow coefficient in the main channel and floodplain using the GA. The proposed formulations were found to have satisfactory accuracy. The coefficient of determination (R^2) and RMSE were 0.93 and 0.060 m/s in the calibration phase and 0.92 and 0.068 m/s in the validation phase, respectively. The high coefficient of determination ensures the reliability of the equations.

$$k_{mc} = (1.096 Dr^{0.0235}) \tag{32}$$

$$k_{fp} = (0.1373 Dr^{0.858}) \tag{33}$$

$$k_s = (1.05416 Dr^{0.774}) \tag{34}$$

Furthermore, Eqs. (35-37) were obtained based on the approach of Abril and Knight(2004) for the main channel and floodplain; the coefficient of determination and RMSE were found to be 0.921 and 0.07 m/s in the calibration phase and 0.902 and 0.098 m/s in the validation phase, respectively.

$$\Gamma_{mc} = 0.802\rho g S_0 H_{mc} Dr \tag{35}$$

$$\Gamma_{fp} = 1.3989\rho g S_0 H_{fp} Dr \tag{36}$$

$$\Gamma_{ms} = 1.5\rho g S_0 H_{ms} Dr \tag{37}$$

Figs. 4 and 5 illustrate the predicted depth-averaged velocities for the three flumes. As can be seen, the optimized secondary flow parameter equations were in good agreement with the observations. The error of the Abril-Knight and Devi-Khatua approaches were 4% and 0.8%, respectively, while that of the Rameshwaran-Shiono approach was 11%.

Figs. 6 and 7 plot the secondary flow coefficient versus the relative depth and width ratio for the main channel, bank slope region, and floodplain. As can be seen, the secondary flow coefficient of the vegetated floodplain was much higher than that of the main channel. This is attributed to higher turbulence, momentum exchange, and vegetation-induced vortices, as mentioned by Rameshwaran and Shiono(2007). According to Fig. 6, a rise in the relative depth led to a slight increase in the

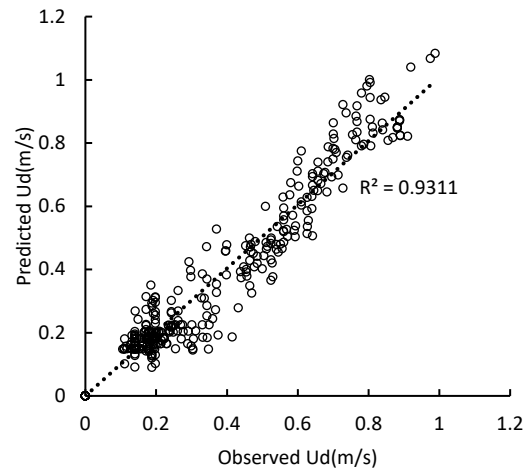


Fig. 4 Comparison of predicted (from Devi and Khatua Optimised equations) and observed depth averaged velocity for all data set.

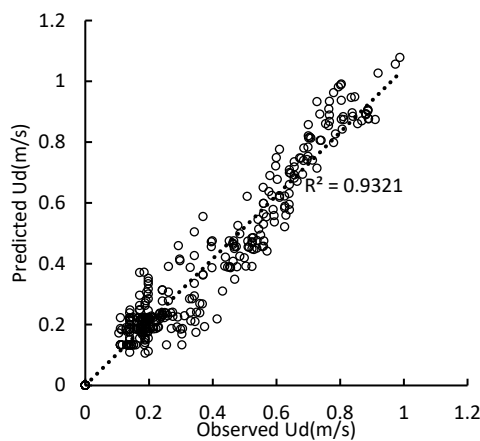


Fig. 5 Comparison of predicted (from Abril and Knight Optimised equations) and observed depth averaged velocity for all data set.

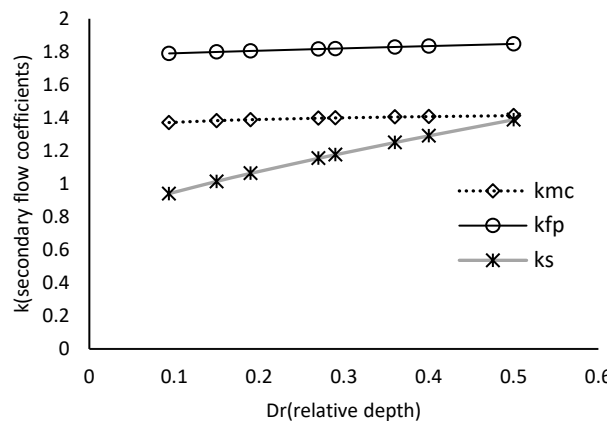


Fig. 6 Variation of secondary flow coefficient in main channel(k_{mc}), floodplain (k_{fp}) and bank slope region (k_s) with relative flow depth.

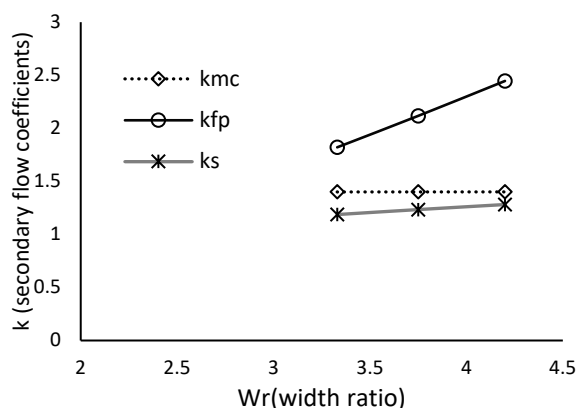


Fig.7 Variation of secondary flow coefficient in main channel (k_{mc}), floodplain (k_{fp}) and bank slope region (k_s) with width ratio.

secondary flow coefficients of the main channel and floodplain, while the coefficient significantly increased as the relative depth increased in the bank slope region. Fig. 7

illustrates the secondary flow coefficients of the main channel, bank slope region and floodplain versus the width ratio. As can be seen, a rise in the width ratio led to no significant change in the secondary flow coefficient of the main channel, however, in the bank slope region, it significantly increased as the width ratio increased. Therefore, it can be said that the secondary flow coefficient is dependent on the flow and geometry of a compound channel. The dependence of the secondary flow on the relative depth and width ratio was also observed in the studies conducted by Devi and Khatua (2017), however, the variation trend is distinct.

Additionally, the secondary flow coefficient was positive in both the main channel and floodplain. Yang et al. (2010) studied the secondary flow coefficient in compound channels and emphasized that the secondary flow sign (UV) could be both positive and negative. In fact, it would be positive under a clockwise rotation and negative under a counterclockwise rotation. As the secondary flow coefficient was positive in the main channel and floodplain, secondary flows are concluded to rotate clockwise. In Figs. 8-10, the predicted and measured depth-averaged velocity and bed shear stress profiles across compound channel were presented. The mean square error (MSE) observed in the estimation of bed shear stress distribution for FCF data using the optimal secondary flow coefficient is 0.02 N/m^2 . This result indicates that the estimated optimal secondary flow coefficient has an acceptable ability in predicting the distribution of bed shear stress. Figs 8-10 show that the predicted and measured depth-averaged velocity and bed shear stress profiles have appropriate consistency in the main channel, main channel mixing layer and floodplain, however, the prediction of t_b and U_d somewhat disagree with the experimental values on the floodplain mixing layer region. This is likely to be due to the applied a generic values of secondary flow coefficient on floodplain which may not be suitable with such region, where a strong interaction develop between the flows in the main channel and on the floodplain. It seems that if the secondary flow coefficient is calculated specifically for the floodplain mixing layer region, the accuracy of the model may be increased.

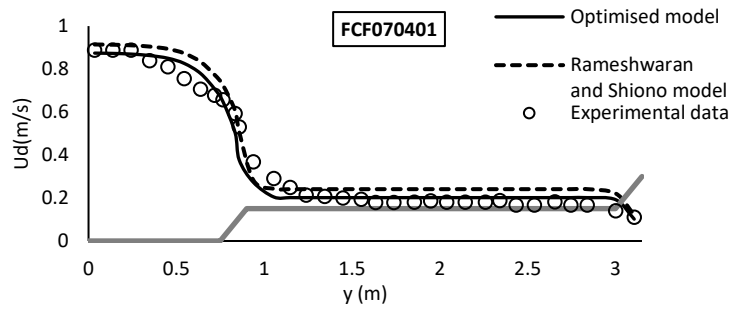


Fig. 8 Comparison of predicted U_d with Rameshwaran and Shiono's experimental data

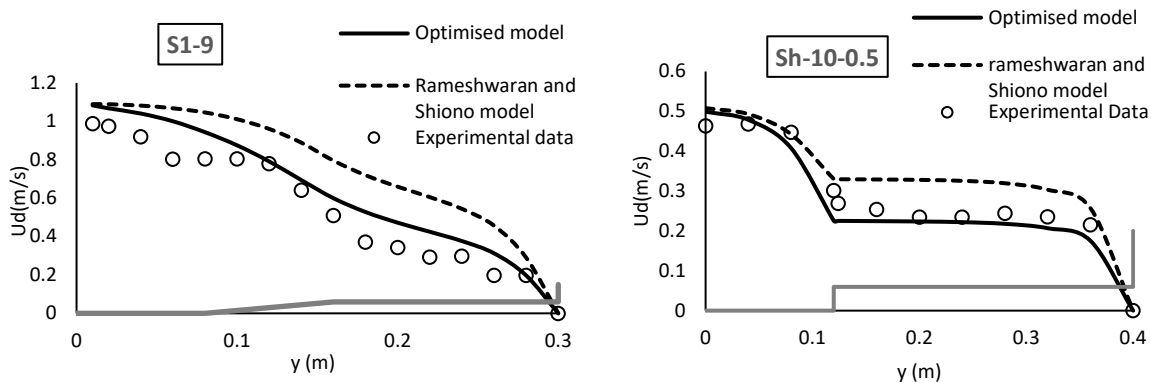


Fig. 9 Comparison of predicted U_d with (a) Mohseni's experimental data and (b) Tavakoli and Mohseni's experimental data.

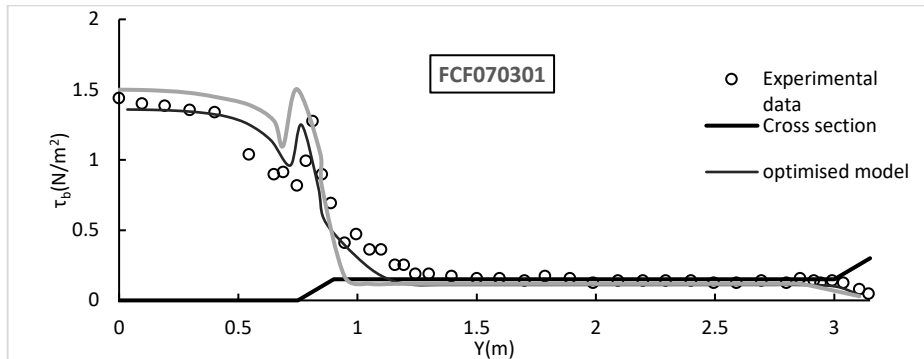


Fig. 10 Comparison of predicted bed shear stress (τ_b) with Rameshwaran and Shiono's experimental data

Fig. 11 represents a linear relationship between the predicted and observed velocities in the main channel and floodplain. As can be seen, the predictions were strongly correlated with the experimental velocities of the main channel; however, the predicted and observed velocities of the floodplain showed a slight difference since the floodplain velocity would be substantially dependent on the position across the channel and vegetation diameter and density. Harris et al. (2003) used a gene programming (GP) algorithm to predict the lateral velocity distribution in a compound channel with a vegetated floodplain and reported the same results.

This study encountered limitations. The governing equation (Eq. (1)) and secondary flow coefficient were formulated for a uniform steady-state flow. Further research is required to implement Eq. (1) under other flow conditions. The proposed equations were developed to estimate the secondary flow induced by rigid, emergent vegetation. Hence, further research is required for flexible, submerged vegetation due to depth velocity profile changes. Finally, the secondary flow distribution may be significantly different for compound channels of an irregular cross-section or a moving bed. Thus, the estimation process should be redesigned for such channels.

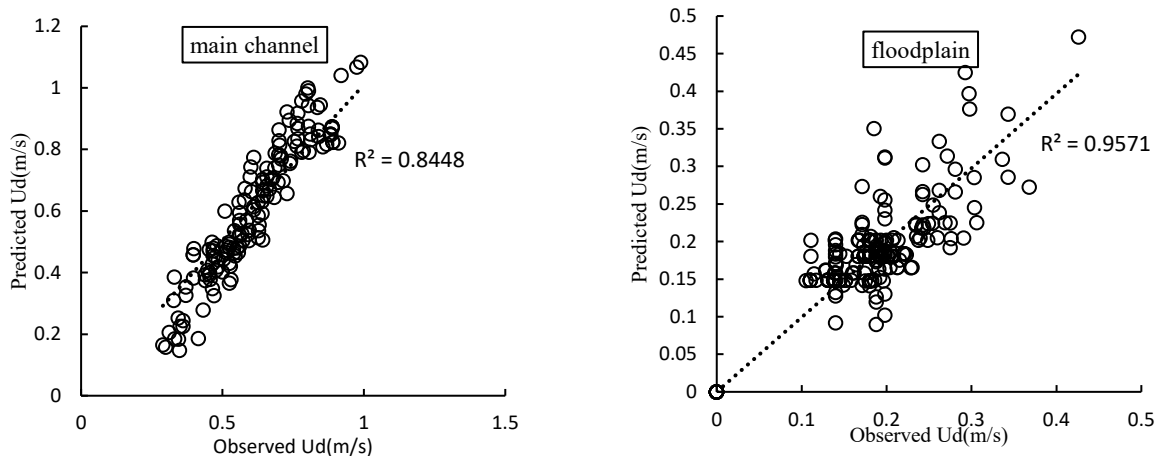


Fig. 11 Regression analysis for depth averaged velocities in main channel and floodplain.

4. Conclusion

This paper employed SKM to estimate the depth-averaged velocity within three compound channels of rectangular and trapezoidal cross-sections with a vegetated floodplain at small and large scales. To solve the SKM, it was required to calculate the friction coefficient, eddy viscosity coefficient, and secondary flow coefficient. The friction coefficient was calculated using the modified Colebrook–White equation. Several eddy viscosity models were adopted to implement the SKM. It was found that the eddy viscosity coefficient had no significant effect on the performance of SKM. The present study focused on calibrating the secondary flow coefficient as it played a key role in the flow simulation of compound channels using SKM. Two approaches were adopted to calibrate the secondary flow coefficient: (1) the approach of Abril and Knight (2004) and (2) the approach of Devi and Khatua (2017). The latter defines the secondary flow coefficient as a function of the relative depth and width ratio. The optimal secondary flow coefficient was obtained using a GA and experimental data for different geometric and hydraulic conditions. A comparison of the predicted and observed velocities demonstrated that the Devi-Khatua calibration method improved the predictive accuracy of SKM by nearly 10.2%. The comparison between modelled and measured profiles of bed shear stress indicates that the estimated optimal secondary flow coefficient has an acceptable ability in predicting the distribution of bed shear stress. These results indicate that secondary flow coefficient is dependent on the relative depth and width

ratio. It was calculated to be positive in both the main channel and floodplain, suggesting clockwise secondary flows. The difference between the observed and predicted velocities was larger on the floodplain than in the main channel, which could have arisen from flow complexities around vegetation.

5. Notation

A_P	Projected area of i plants per unit volume
A_v	Average cross-sectional area of i vegetation stem
B	Half floodplain bed width
b	Half main channel bed width
C_D	Drag coefficient
D_v	Rod diameter
Dr	Relative flow depth
H	Water depth
h	Bankfull depth
F_D	Drag force per unit fluid volume for i vegetation
f	Darcy–Weisbach friction factor
g	Gravitational acceleration
k_s	Roughness height
N_v	Averaged i vegetation density
n	Manning coefficient
R	Hydraulic Radius
Re	Local Reynolds number
Re_{rod}	Rod Reynolds number
s	Side slope of the banks (1: s —vertical : horizontal)
S_o	Channel bed slope
S_F	Shading factor
s_f	Floodplain side wall slope distance
s_m	Main channel side wall slope distance
U, V, W	Mean velocity components in the x, y and z coordinate directions
U^*	Friction velocity
U_d	Depth-averaged velocity
x, y, z	Coordinate directions

Greek letters

\mathcal{F}	Advection term
α	Porosity
β	Eddy viscosity coefficient
δ	Width of the mixing layer
κ	Von Karman constant
λ	Eddy viscosity coefficient
ν	Kinematic viscosity
ν_t	Depth-averaged eddy viscosity
ρ	Density
τ_b	Bed shear stress
<i>Subscript</i>	
d	depth-averaged value
fp	floodplain
mc	main channel

6. References

- Abril, J. & Knight, D. (2004). Stage-discharge prediction for rivers in flood applying a depth-averaged model. *J. Hydraul. Res.*, 42(6), 616–629.
- Ackers, P. (1991). Hydraulic design of straight compound channels. Hydraulics Research Ltd., Wallingford.
- Alawadi, W., Al-Rekabi, W.S. & Al-Aboodi, A.H. (2018). Application of the Shiono and Knight Method in asymmetric compound channels with different side slopes of the internal wall. *Appl. Water Sci.* 8(4), <https://doi.org/10.1007/s13201-018-0663-4>.
- Bousmar, D. & Zech, Y. (2004). Velocity distribution in non-prismatic compound channels. In: *Proceedings of the Institution of Civil Engineers-Water Management*, 157(2), 99-108.
- Das, B.S., Khatua, K.K. & Devi, K. (2018). Application of Lateral Distribution Method and Modified Lateral Distribution Method to the Compound Channel Having Converging Floodplains. In: *Proceedings of the International Conference on Microelectronics, Computing and Communication Systems*, 293-303.
- Devi, K. & Khatua, K. (2017). Depth-averaged velocity and boundary shear stress prediction in asymmetric compound channels. *Arab J Sci Eng.* 42(9), 3849–3862.
- Han, L.J., Zeng, Y.H., Chen, L. & Huai, W.X. (2016). Lateral velocity distribution in open channels with partially flexible submerged vegetation. *Environ. Fluid Mech.*, 16(6), 1267-1282.
- Harris, E.L., Babovic, V. & Falconer, R.A. (2003). Velocity predictions in compound channels with vegetated floodplains using genetic programming. *International Journal of River Basin Management*, 1(2), 117-123.
- Huai, W., Gao, M., Zeng, Y. & Li, D. (2009). Two-dimensional analytical solution for compound channel flows with vegetated floodplains, *Appl. Math. Mech.-English Ed.*, 30, 1121-1130.
- Knight, D. & Abril, C.J. (1996). Refined calibration of a depth-averaged model for turbulent flow in a compound channel. *Proc Inst Civ Eng Water Marit Energy*, 118(3), 151–159.
- Knight, D.W. & Shiono, K. (1996). River channel and floodplain hydraulics. In: *Floodplain Processes*, Anderson, M.G., Walling, D.E., Bates, P.D., eds., Chichester: Wiley, 139-181.
- Knight, D.W. & Hamed, M.E. (1984). Boundary shear in symmetrical compound channels. *J. Hydraul. Eng.*, 110(10), 1412–1430.
- Knight, D.W., Yuen, K.W.H. & Alhamid, A.A.I. (1994). Boundary shear stress distributions in open channel flow. In: *Physical mechanisms of mixing and transport in the environment*, Beven, K., Chatwin, P. and Millbank, J., eds., Wiley, New York, 51–87.
- Lashkar Ara, B. & Dehghani, I. (2016). Calibration of Shiono and Knight Model to Estimate Shear Stress for Trapezoidal Channel. *Irrigation Sciences and Engineering*, 38(4), 189-201.
- Liu, C., Luo, X., Liu, X. & Yang, K. (2013). Modeling depth-averaged velocity and bed shear stress in compound channels with emergent and submerged vegetation. *Advances in Water Resources*, 60, 148-159.
- Mohseni, M., Samani, J.M. & Ayyubzadeh, S.A. (2013). Depth-averaged Velocity Distribution in Compound Channel with Vegetated Floodplains. *Journal of Hydraulics*, 8(3), 63-75. (In Persian)
- Mohseni, M. (2015). Development a 2D Suspended Load Transport in Non-Submerged, Rigid Vegetated Floodplain of Compound Channel, Ph.D thesis, Tarbiat Modares University, Tehran, Iran.
- Nepf, H. (1999). Drag, Turbulence and Diffusion in Flow Through Emergent Vegetation. *Water Resources Research*, 35, 479–489.
- Pasche, E. & Rouve, G. (1985). Overbank flow with vegetatively roughened flood plains., *Journal of Hydraulic Engineering*, 111,1262.
- Posey, C.J. (1967). Computation of discharge including over-bank flow. *Civ. Eng.*, 37(4), 62–63.

- Pu, J.H., Hussain, A., Guo, Y.K., Vardakastanis, N., Hanmaiahgari, P.R. & Lam, D. (2019). Submerged flexible vegetation impact on open channel flow velocity distribution: An analytical modelling study on drag and friction. *Water Science and Engineering*, 12(2), 121-128.
- Rajaratnam, N. & Ahmadi, R.M. (1979). Interaction between main channel and floodplain flows. *J. Hydr. Div.*, 105(5), 573-588.
- Rameshwaran, P. & Shiono, K. (2007). Quasi two-dimensional model for straight overbank flows through emergent., *J Hydraul Res*, 45(3), 302-315.
- Sellin, R.H.J. (1964). A laboratory investigation into the interaction between the flow in the channel of a river and that is over its floodplain. *Houille Blanche*, 7, 793-802.
- Shiono, K., Takeda, M., Yang, K., Sugihara, Y. & Ishigaki, T. (2012). Modeling of vegetated rivers for inbank and overbank flows, Proceedings of the International Conference on Fluvial Hydraulics, San Jose, Costa Rica, 263 - 269.
- Shiono, K. & Knight, D. (1991). Turbulent open-channel flows with variable depth across the channel. *J Fluid Mech*, 222, 617-646.
- Shiono, K. & Knight, D.W. (1990). Mathematical models of flow in two or multi stage straight channels. In: Proceedings of the International Conference on River Flood Hydraulics. New York: John Wiley & Sons, 229-238.
- Sun, X.K. & Shiono, K. (2008). Modelling of velocity and boundary shear stress for one-line vegetation along the edge of floodplain in compound channel, ICHE, Nagoya.
- Sun, X. & Shiono, K. (2009). Flow resistance of one-line emergent vegetation along the floodplain edge of a compound open channel., *Adv Water Resour*, 32(3), 430-438.
- Sun, X., Shiono, K., Fu, X.Y., Yang, K.J. & Huang, T.L. (2013). Application of Shiono and Knight method to compound open channel flow with one-line emergent vegetation. In Advanced Materials Research, *Trans Tech Publications Ltd.*, 663, 930-935.
- Tang, X.N. & Knight, D.W. (2009). Lateral distributions of streamwise velocity in compound channels with partially vegetated floodplains., *Science in China Series E: Technological Sciences*, 52(11), 3357-3362.
- Tavakoli., F. & Mohseni, M. (2020). Experimental Study of Vertical velocity profiles in compound channels with vegetation on floodplains. *Journal of Hydraulics*, 15(4), 31-45. (In Persian)
- Tominaga, A. & Knight, D.W. (2006). Numerical evaluation of secondary flow effects on lateral momentum transfer in overbank flows. In: Proceedings of the International Conference on Fluvial Hydraulics. London: Taylor & Francis, 353-361.
- Yang, W. & Choi, S.U. (2010). A two-layer approach for depth-limited open channel flows with submerged vegetation. *J. Hydraul. Res.*, 48(4), 466-475.
- Yang, K., Cao, S. & Knight, D.W. (2007). Flow patterns in compound channels with vegetated floodplains. *Journal of Hydraulic Engineering*, 133(2), 148-159.
- Zahiri, A, Tang, X. & Sharifi, S. (2017). Optimal prediction of lateral velocity distribution in compound channels, *International Journal of River Basin Management*, 15(3), 1-7.
- Zheleznyakov, G.V. (1971). Interaction of channel and floodplain streams. Proc., Int. Association for Hydraulic Research Congress, Paris, 5, 144-148.